INTERNATIONAL JOURNAL FOR NUMERICAL METHODS IN FLUIDS
Int. J. Numer. Meth. Fluids 2001; **35**: 395–420

A multigrid method with higher-order discretization schemes

Agamemnon A. Varonos and George C. Bergeles*,[1]

Laboratory of Aerodynamics, Fluids Section, Department of Mechanical Engineering, National Technical University of Athens, Athens, Greece

SUMMARY

The implementation of the multigrid method into the SIMPLE algorithm presents interesting aspects concerning the mass fluxes conservation on coarser grids, the $k-\varepsilon$ turbulence model and the higher-order discretization schemes. Higher-order discretization schemes for the convection terms are increasingly used in order to guarantee accuracy in demanding engineering applications. However, when used in single-grid algorithms, their convergence is considerably slower compared with the first-order schemes. Unbounded higher-order schemes offer maximum accuracy, but quite often they do not converge due to their oscillatory behaviour. This paper demonstrates the dual function of the multigrid method: reduction of CPU time and stabilization of the iterating procedure, making it possible to perform computations with the third-order accurate QUICK scheme in all cases. The method is applied to the calculation of two- and three-dimensional flows with or without turbulence modelling. The results show that the convergence rate of the present algorithm does not deteriorate when QUICK is used and that, if applied on complex engineering cases, large gains in computational time can be achieved. Copyright © 2001 John Wiley & Sons, Ltd.

KEY WORDS: convergence rate; higher-order schemes; multigrid; numerical accuracy; SIMPLE

1. INTRODUCTION

The increase of computer power over the last two decades has permitted the application of computational fluid dynamics (CFD) methods to a significant number of engineering flows. These are, generally, high-Reynolds number flows, extending to complex computational domains, which often incorporate different length scales. In such flows, the numerical modelling of the incompressible Navier–Stokes equations requires fine computational grids, with costs in computer memory and run time. One way to decrease the computational costs is

* Correspondence to: Laboratory of Aerodynamics, Fluids Section, Department of Mechanical Engineering, National Technical University of Athens, 9 Heroon Polytechniou Ave., 15 773, Athens, Greece. Tel.: + 30 1 7721058, 7721056; fax: + 30 1 7721057.
[1] E-mail: bergeles@fluid.mech.ntua.gr

Received August 1999
Revised February 2000

Copyright © 2001 John Wiley & Sons, Ltd.

the use of higher-order schemes for the convective terms discretization. Higher-order schemes, such as QUICK [1], SMART [2], VONOS [3] or BSOU [4], allow coarser domain discretization, resulting in lower computer time and memory requirements for the same level of accuracy [3].

A second way to reduce the run time of a Navier–Stokes algorithm is to improve the solver or the equation formulation itself. The application of a preconditioned conjugate gradient method [5,6] offers some advantages, but its monotonic behaviour as the grid size increases is not guaranteed. On the other hand, the multigrid method is generally considered as the most powerful tool to reduce the computational effort. The multigrid method is based on the observation that the numerical solution of equations on coarse grids is quite fast, while, as the grid density increases, it becomes progressively slower. This is due to the fact that high frequency error components are smoothed rapidly on fine grids. However, low frequency error components are those that are responsible for the convergence delay, because their optimal smoothness rate should be achieved on coarser grids. According to this observation, the principle of the multigrid method is to cut the lower frequencies of error components on coarser grids, while the high frequency components of the fine grid are smoothed out rather than being solved iteratively. The most attractive characteristic of the multigrid method compared with other convergence acceleration techniques is that its convergence rate is independent of the finest grid size, and that the amount of computational effort needed to solve a system of N unknowns, is proportional to N [7].

Up to now the development and application of multigrid methods has been demonstrated mainly on simple two-dimensional cases; the most common being the lid-driven cavity flow [8–11]. These studies, except the one of Vanka [10], concern the implementation of the multigrid method into the SIMPLE [12] algorithm. Lien and Leschziner [8] implemented the k–ε turbulence model into the multigrid algorithm, which was applied to a two-dimensional plane diffuser. Recently, three-dimensional multigrid algorithms have been developed by Dick and Steelant [13] and Drikakis *et al.* [14], combined with a flux-splitting and an artificial compressibility formulation respectively. The relevant test cases concern three-dimensional turbulent compressible flows and laminar incompressible flows. However, up to now very few or no papers—to the authors' knowledge—deal with the application of the multigrid method on three-dimensional incompressible turbulent flows, solved with the SIMPLE algorithm.

The aim of this paper is to not only present a multigrid application on a rather complicated flow field, but also to examine the influence of the multigrid convergence characteristics on higher-order discretization schemes. The interaction of the multigrid method with the higher-order discretization schemes showed that the integration of these procedures does not present stability problems. Higher-order discretization schemes have already been used in some of the above-mentioned papers. However, the most important finding of the present study (not previously reported) is that the multigrid method allows the unconditional use of unbounded higher-order schemes, such as QUICK [1]. This means that now unbounded discretization schemes can be employed even in cases where convergence of the iterative procedure was prohibited by the well-known oscillatory behaviour of these schemes. Relevant work on this subject has been recently published by Oosterlee *et al.* [15], who focused on the development of multigrid line smoothers for *bounded* schemes only. The smoothers were developed on the basis of the flux-splitting formulation and the test cases included the two-dimensional lid-driven cavity flow and an inviscid channel compressible flow problem.

Copyright © 2001 John Wiley & Sons, Ltd.

The following sections present the most important aspects of the implementation of the multigrid method into the SIMPLE algorithm, as well as the specific formulations adopted for the $k-\varepsilon$ turbulence model and the higher-order schemes. The present algorithm has been applied on two two-dimensional cases and one three-dimensional case, with increased complexity. The two-dimensional cases include the above-mentioned and well-documented lid-driven cavity flow [16] and the backward-facing step case [17] (turbulent flow); the three-dimensional one concerns the turbulent flow around a cube [18]. The presentation of the numerical results focuses on the convergence acceleration and the parameters affecting it, without neglecting the most interesting flow characteristics of each case.

2. DISCRETIZATION METHOD

The continuity and momentum equations in tensor formulation are:

$$\frac{\partial}{\partial x_j}(\rho u_j) = 0, \quad j = 1, 2, 3 \tag{1}$$

$$\frac{\partial}{\partial x_j}\left(\rho u_j u_i - \mu \frac{\partial u_i}{\partial x_j}\right) = -\frac{\partial P}{\partial x_i} + \frac{\partial}{\partial x_j}\left[\mu\left(\frac{\partial u_j}{\partial x_i}\right)\right] \tag{2}$$

where ρ is the density, u_i and x_i are the Cartesian velocity components and co-ordinate directions respectively, P is the pressure and μ denotes the dynamic viscosity.

The transport equations for the turbulent kinetic energy k and its dissipation rate ε ($k-\varepsilon$ model [19]) are

$$\frac{\partial}{\partial x_j}\left(\rho u_j k - \frac{\mu_t}{\sigma_k}\frac{\partial k}{\partial x_j}\right) = G - \rho\varepsilon \tag{3}$$

$$\frac{\partial}{\partial x_j}\left(\rho u_j \varepsilon - \frac{\mu_t}{\sigma_\varepsilon}\frac{\partial \varepsilon}{\partial x_j}\right) = \frac{C_1 \varepsilon G - C_2 \rho \varepsilon^2}{k} \tag{4}$$

with

$$\mu_t = \frac{\rho C_\mu k^2}{\varepsilon}, \quad C_\mu = 0.09 \tag{5}$$

G is the turbulent shear stress production, expressed as

$$G = \mu_t \frac{\partial}{\partial x_j}\left(\frac{\partial u_i}{\partial x_j} + \frac{\partial u_j}{\partial x_i}\right)\frac{\partial u_i}{\partial x_j} \tag{6}$$

The $k-\varepsilon$ model constants are $C_1 = 1.44$, $C_2 = 1.92$, $\sigma_k = 0.9$ and $\sigma_\varepsilon = 1.3$.

Copyright © 2001 John Wiley & Sons, Ltd.

The values of the dependent variables u_i and P are stored in the centre of the computational grid cells in a collocated arrangement. The transport equations (1)–(4) are then integrated over the finite control volume (Figure 1), which surrounds the storage locations and coincides with the grid lines (lowercase subscripts refer to quantities on the cell face, whereas uppercase subscripts refer to quantities on the cell centres). The complete procedure is described in Varonos and Bergeles [3] and yields

$$A_P\phi_P = A_E\phi_E + A_W\phi_W + A_N\phi_N + A_S\phi_S + A_U\phi_U + A_D\phi_D + S_\phi \cdot \mathrm{Vol} + SU_x + SU_y + SU_z \tag{7}$$

where

$$\phi = u_i,\ P,\ k,\ \varepsilon \tag{8}$$

$$A_P = A_E + A_W + A_N + A_S + A_U + A_D \tag{9}$$

and

$$A_E = \max(0,\ -C_e) + D_e, \qquad A_W = \max(0,\ C_w) + D_w \tag{10}$$

$$\begin{aligned} SU_x = {} & \max(0,\ C_e)\mathrm{DWF}_e^+(\phi_P - \phi_E) + \max(0,\ -C_e)\mathrm{DWF}_e^-(\phi_P - \phi_E) \\ & + \max(0,\ C_w)\mathrm{DWF}_w^+(\phi_P - \phi_W) + \max(0,\ -C_w)\mathrm{DWF}_w^-(\phi_P - \phi_W) \end{aligned} \tag{11}$$

S_ϕ is the source term. The downwind weighting factor (DWF) [20] in Equation (11) is defined as

$$\mathrm{DWF} = \frac{\phi_e - \phi_P}{\phi_E - \phi_P} \tag{12}$$

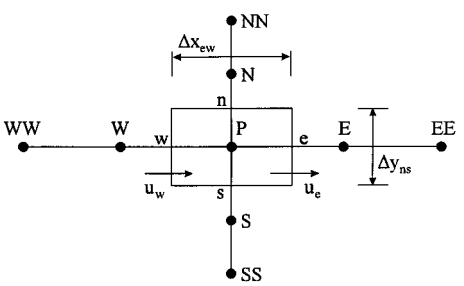

Figure 1. Control volume annotation.

Copyright © 2001 John Wiley & Sons, Ltd.

where ϕ_e is the value on the eastern face of the cell, as it is given by the discretization scheme [3]. The superscripts $+$ and $-$ over the DWF indicate the direction of the u-velocity. The DWFs have to be calculated according to its sign.

The diffusion coefficients and the mass fluxes across the cell faces are computed as follows:

$$D_e = [\Gamma_\phi]_e \frac{\Delta y_{ns} \Delta z_{ud}}{\Delta x_{EP}}, \qquad D_w = [\Gamma_\phi]_w \frac{\Delta y_{ns} \Delta z_{ud}}{\Delta x_{PW}} \tag{13}$$

$$C_e = [\rho u]_e \Delta y_{ns} \Delta z_{ud}, \qquad C_w = [\rho u]_w \Delta y_{ns} \Delta z_{ud} \tag{14}$$

The interpolation of the velocity on the cell faces requires special treatment, because the collocated storage of variables causes the decoupling of velocities and pressure. This in turn produces oscillations in the pressure field. The oscillations may be damped by the introduction of a fourth-order pressure derivative into the continuity equation, which in the Rhie and Chow [21] equivalent expression gives

$$u_e = \overline{(u_E, u_P)}\Big|_e + \overline{\left(\frac{\mathrm{Vol}}{A_P} \frac{\partial P}{\partial x}\Big|_E, \frac{\mathrm{Vol}}{A_P} \frac{\partial P}{\partial x}\Big|_P \right)}\Big|_e - \overline{\left(\frac{\mathrm{Vol}}{A_P}\Big|_E, \frac{\mathrm{Vol}}{A_P}\Big|_P \right)}\Big|_e \frac{P_E - P_P}{\Delta x_{EP}}$$

or

$$u_e = \bar{u}\big|_e + \overline{\frac{\mathrm{Vol}}{A_P} \frac{\partial P}{\partial x}}\Big|_e - \overline{\frac{\mathrm{Vol}}{A_P}}\Big|_e \frac{\partial P}{\partial x}\Big|_e \tag{15}$$

where u_e is the approximation of the u-velocity on the eastern cell face, before the pressure correction, and Vol is the volume of the computational cell. The $\overline{(\ ,\ )}$ symbol denotes interpolation on the cell face. The same relations expressed in the y- and z-directions apply for the rest of the coefficients. The system of the discretized equations is then solved iteratively using the SIMPLE algorithm [12], incorporating a fast line-by-line solver.

3. MULTIGRID METHOD

The procedure described in the previous section corresponds to a single-grid algorithm. It is quite fast in the first iterations but much slower thereafter, and the convergence rate deteriorates as the grid is refined. This behaviour can be explained by a Fourier analysis of the error components [7]. The iterative procedure smoothes very efficiently the error wavelengths with size comparable with the computational cells size, while it is inefficient to annihilate the lower frequency components. According to this observation it is advantageous to smooth each error frequency component on a grid with the appropriate line spacing. The multigrid technique combines this concept with an information exchange between the flow properties, so that low frequency components of the error are smoothed out in coarser grids, while the coarse grid information is transferred to the finer grids.

When Equation (7) is satisfied, it may be written as

Copyright © 2001 John Wiley & Sons, Ltd.

$$[\mathscr{A}_m]\{\varphi_m\} = \{\mathscr{S}_m\} \tag{16}$$

where m is the grid number, $[\mathscr{A}_m]$ is the coefficient matrix, $\{\mathscr{S}_m\}$ is the source term vector and $\{\varphi_m\}$ is the exact solution vector. Note that in the present annotation, $m = 1$ corresponds to the finest grid, on which is sought the numerical solution of Equation (7).

After n_m iterations with the SIMPLE algorithm on this grid, the approximate solution $\{\phi_m\}$ satisfies the following residual equation:

$$\{R_m\} = \{S_m\} - [A_m]\{\phi_m\} \tag{17}$$

$[A_m]$ and $\{S_m\}$ are current approximations of $[\mathscr{A}_m]$ and $\{\mathscr{S}_m\}$, based on the approximate solution $\{\phi_m\}$ and $\{R_m\}$ is the residual of Equation (7). The multigrid coupling equation is derived by subtracting Equation (17) from Equation (16)

$$[\mathscr{A}_m]\{\varphi_m\} = \{\mathscr{S}_m\} + [A_m]\{\phi_m\} - \{S_m\} + \{R_m\} \tag{18}$$

Equation (18) is transferred to the next coarser grid $m+1$ as follows:

$$[\hat{A}_{m+1}]\{\hat{\phi}_{m+1}\} = \{\hat{S}_{m+1}\} + \underbrace{[\tilde{A}_{m+1}]\{\tilde{\phi}_{m+1}\} - \{\tilde{S}_{m+1}\} + \{\tilde{R}_{m+1}\}}_{\text{constant term}} \tag{19}$$

The $\hat{(\ )}$ symbol is attributed to operators and variables that are modified during the iterations on the coarser grid $m+1$. The $\{\tilde{\ }\}$ symbol represents vectors that have been transferred from grid m to grid $m+1$ by a procedure widely known as 'restriction'. Figure 2 shows the control volumes of the fine and coarse grids. Coarser grids are generated simply by assembling four of the fine grid cells. This is done to simplify coarser grid generation, but imposes some restrictions on the selection of the grid nodes number, as well as it does for the solid

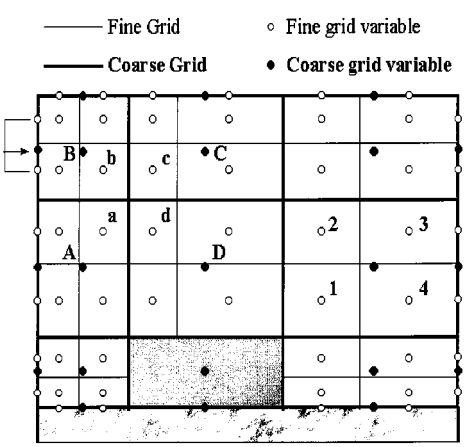

Figure 2. Multigrid arrangement and storage locations.

Copyright © 2001 John Wiley & Sons, Ltd.

boundaries definition. Restriction is made with bilinear interpolations of the four fine grid variables surrounding a coarse grid value and it is denoted by the operator I_m^{m+1}

$$\tilde{\phi}_{m+1} = I_m^{m+1}\phi_m \tag{20}$$

The multigrid method can also be used with an arbitrary selection of the coarser grids sizes. This choice should be employed in engineering problems with complex boundaries because it complicates further the computer algorithm and requires the storage of the connectivity between the coarse and fine grid variables. Connectivity information is necessary for the restriction procedure and in the present formulation, it is straightforwardly deduced by the assembly of the four fine grid cells.

The restriction of the residual $\{\tilde{R}_{m+1}\}$ is done by summing the residuals of the four fine grid control cells (Figure 2)

$$\tilde{R}_{m+1} = R_m^1 + R_m^2 + R_m^3 + R_m^4 \tag{21}$$

On the other hand, for consistency reasons, the computation of $[\tilde{A}_{m+1}]$ and $\{\tilde{S}_{m+1}\}$ is done in the same way as it is done for $[\hat{A}_{m+1}]$ and $\{\hat{S}_{m+1}\}$, based on the values of $\tilde{\phi}_{m+1}$ (for more details see Hortmann *et al.* [22]). At the first iteration on the coarse grid, $\tilde{\phi}_{m+1}$ and $\hat{\phi}_{m+1}$ are identical. In subsequent iterations, the terms in the bracket (Equation (19)) remain constant and are introduced as a source term in the general set of matrices of Equation (7).

The mass fluxes, used to evaluate $[\hat{A}_{m+1}]$ before the first iteration on the coarse grid, are conservatively evaluated by summing the fine grid mass fluxes through the corresponding control volume faces (Figure 3). During the coarse grid iterations, the mass fluxes calculation has to be consistent with the multigrid procedure, and therefore the former are corrected as follows:

$$\hat{C}_e|_{m+1} = \tilde{C}_e|_{m+1} + \rho_e|_{m+1}\Delta y_{ns}\Delta z_{ud}(\hat{u}_e|_{m+1} - \check{u}_e|_{m+1}) \tag{22}$$

where $\hat{u}_e|_{m+1}$ and $\check{u}_e|_{m+1}$ are calculated according to Equations (23) and (24)—which have forms similar to Equation (15)—as

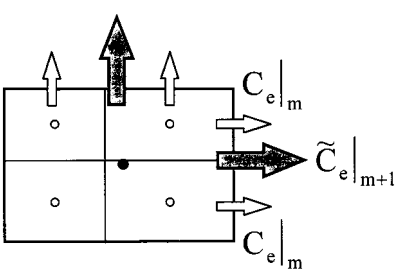

Figure 3. Mass fluxes restriction.

Copyright © 2001 John Wiley & Sons, Ltd.

$$\hat{u}_e|_{m+1} = \left[\bar{\tilde{u}}|_e + \left. \frac{\overline{\mathrm{Vol}}}{\hat{A}_P} \frac{\partial P'}{\partial x} \right|_e - \left. \frac{\overline{\mathrm{Vol}}}{\hat{A}_P} \right|_e \left. \frac{\partial P'}{\partial x} \right|_e \right]_{m+1} \tag{23}$$

$$\check{u}_e|_{m+1} = \left[\bar{\tilde{u}}|_e + \left. \frac{\overline{\mathrm{Vol}}}{\hat{A}_P} \frac{\partial P'}{\partial x} \right|_e - \left. \frac{\overline{\mathrm{Vol}}}{\hat{A}_P} \right|_e \left. \frac{\partial P'}{\partial x} \right|_e \right]_{m+1} \tag{24}$$

where P'_{m+1} is a coarse grid *pressure correction*, as explained in Section 3.1.

The multigrid coupling is completed with the transfer of the coarse grid corrections to the fine grid solution, according to the full approximation scheme (FAS) [23]

$$\phi_m^{\mathrm{new}} = \phi_m^{\mathrm{old}} + I_{m+1}^m (\hat{\phi}_{m+1} - \tilde{\phi}_{m+1}) \tag{25}$$

I_{m+1}^m is the 'prolongation' operator, which transfers the coarse grid corrections $(\hat{\phi}_{m+1} - \tilde{\phi}_{m+1})$ to the fine grid by means of bilinear interpolations. The I_{m+1}^m operator transfers the corrections of four coarse grid points (A to D) to each of the fine grid storage locations (a to d in Figure 2).

3.1. Coarse grid pressure correction

The above procedure results from the application of the FAS, which has been developed for non-linear $[A]$ operators; therefore, it is applied on the momentum equations only. Although the FAS is applicable to linear operators as well, it is not used for the continuity equations. In SIMPLE, continuity is used to form the pressure correction equation and since the pressure operator $[A]$ is also linear, it is advantageous to use the multigrid correction scheme [7]. A second reason to use the correction scheme instead of the FAS is that pressure in SIMPLE is built up by summing pressure corrections rather than being solved directly, as it is done for the velocity components of the momentum equations [22,23]. According to the correction scheme, it is not necessary to restrict the fine grid pressure field to the coarse grid. What has to be done is to compute a *pressure correction* for the fine grid, which is denoted by P'_{m+1}. Thus, the coarse grid procedure for the *pressure correction* is as follows:

First it is set:

$$\{P'_{m+1}\} = 0 \tag{26}$$

The coarse grid continuity equation provides a *correction* to the *pressure correction* P'_{m+1}, which is calculated by the equation

$$[\hat{A}_{m+1}]\{P''_{m+1}\} = \{R'_{m+1}\} \tag{27}$$

where the coarse grid mass residual is computed by the flux balance in each computational cell

$$R'_{m+1} = -\hat{C}_e|_{m+1} + \hat{C}_w|_{m+1} - \hat{C}_n|_{m+1} + \hat{C}_s|_{m+1} - \hat{C}_u|_{m+1} + \hat{C}_d|_{m+1} \tag{28}$$

Once Equation (27) is solved, P'_{m+1} is corrected as

Copyright © 2001 John Wiley & Sons, Ltd.

$$P'^{\,\mathrm{new}}_{m+1} = P'^{\,\mathrm{old}}_{m+1} + P''_{m+1} \tag{29}$$

and as soon as the iterative procedure in the coarse grid is completed, the coarse grid pressure correction is transferred to the fine grid with the same prolongation operator I^m_{m+1} (Equation (25))

$$P^{\mathrm{new}}_m = P^{\mathrm{old}}_m + I^m_{m+1} P'_{m+1} \tag{30}$$

3.2. Boundary conditions

The stability and efficiency of the multigrid method is significantly affected by the boundary conditions, which have to be consistent with the procedure described in the previous sections. Dirichlet conditions of the fine grid have to be also restricted to the coarse grid. In the case of two-dimensional flow, restriction is made by linear interpolation (Figure 2).

The mass balance procedure at the flow field exit is slightly more complicated. No restriction nor prolongation is required and the mass balance calculation for the u-velocity component is made on the finest grid only. The same is valid for the application of the exit Neumann conditions on the two other velocity components v and w.

The application of Neumann boundary conditions at other sections of the flow field (e.g. at the top boundary) is kept unmodified for the fine and coarse grids. A more accurate approach would be first to restrict the fine grid variables to the coarse one and then apply directly the Neumann condition before iterations start on the coarse grid. Although this implementation is mathematically consistent [23], it increases programming complexity. Numerical trials that were carried out in the present study showed that this choice does not improve significantly the algorithm's efficiency and that it is advantageous to employ the unmodified Neumann conditions, as it is suggested by Hänel *et al.* [24].

3.3. Turbulence modelling

The direct application of the multigrid method on Equations (3) and (4) generates negative values for k and ε, leading then to a breakdown of the calculation [8,23]. Dick and Steelant [13] used a damping procedure proposed by Lien and Leschziner [8], which stabilizes the k–ε multigrid procedure and accelerates the convergence rate. However, the solution of the k–ε transport equations on the coarse grid and their prolongation to the fine grid are time consuming. Therefore, in the present work, the k–ε equations are solved on the finest grid only and their values are restricted to the coarse one, where the turbulent viscosity μ_t is computed once, according to Equation (5). The wall functions calculation is the same for every grid level. This choice is proved to be quite efficient, especially with large (finest) computational grids.

3.4. Higher-order discretization schemes

The use of higher-order discretization schemes has been recently imposed by the need to acquire accurate results in a wide range of engineering flows. In a single grid algorithm, bounded higher-order discretization schemes, such as SMART [2], VONOS [3] or BSOU [4], present much lower convergence rates than the ones obtained by the well-known Hybrid

Copyright © 2001 John Wiley & Sons, Ltd.

scheme [25]. On the other hand, higher-order schemes are much more time efficient than the Hybrid one, because they achieve the same level of accuracy with significantly fewer computational points [3].

QUICK [1] is a well-known third-order accurate scheme, which in a number of studies was proven to give the most accurate results. However, QUICK lacks the boundedness property and therefore it often creates further delays in convergence or does not converge at all. This led to the development of bounded versions of QUICK (e.g. VONOS [3]), which are used as higher-order schemes in single grid algorithms, without stability problems. The development of the present algorithm led to the conclusion that the multigrid method not only stabilizes and increases the convergence rate of bounded schemes, but that it does so unconditionally for the QUICK scheme as well.

The implementation of the higher-order scheme in the multigrid procedure is done in two ways: in the first one, the higher-order scheme is applied on the finest grid only, whereas the Hybrid scheme is used for the coarser grids discretization. This approach saves computational time within the multigrid cycle and it is advantageous when employed with high-Reynolds number turbulent flows. The second approach consists of applying the higher-order scheme on all grid levels. This choice does not create stability problems and increases the convergence rate of the multigrid procedure for laminar two-dimensional problems.

3.5. Multigrid cycles

The method presented in the previous sections describes a two-grid algorithm, where properties and residuals are transferred from the fine to the coarse grid. According to the multigrid concept, this procedure can be extended to more grid levels, depending on the number of nodes of the finest grid. Optimum convergence rates are obtained with three to five grid levels.

For the grid level sequence (Figure 4), the V-cycle is adopted. Two types of V-cycles have been investigated. The first has a constant number of iterations at all grid levels, between the restriction and prolongation procedures, and is denoted as $[l_r, l_p]$ (Figure 4(a)). The second uses the function $m + l$, where m is the current grid level and l is a constant number of iterations (Figure 4(b)). This cycle—denoted $[m + l_r, m + l_p]$—lets more iterations be performed on the coarser grids and less on the finer ones ($m = 1$ is the finest grid). This is done because iterations on coarse grids are faster, providing a quick decrease of the residual.

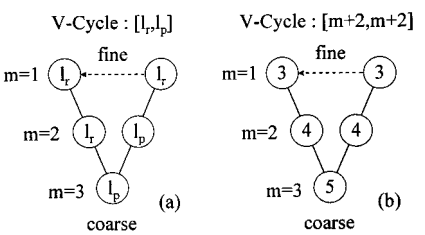

Figure 4. V-cycle types: (a) constant number of iterations before restriction and prolongation, (b) most iterations are performed on coarse grids.

Copyright © 2001 John Wiley & Sons, Ltd.

The full multigrid approach [22], in which the solution of the field starts on the coarsest grid and then it is advanced with successive multigrid cycles to the finest level, was not adopted in the present work.

4. TEST CASES AND RESULTS

The multigrid algorithm described in the previous sections has been applied on three different test cases with increased complexity. The lid-driven cavity test flow [16] (two-dimensional) was used to initially investigate the performance of the algorithm and to optimize the parameters of the multigrid method. The second case is the two-dimensional turbulent flow over a backward-facing step [17], which served to assess the method in conjunction with the $k-\varepsilon$ model. The turbulent flow around a cube [18] is finally simulated in order to verify that convergence characteristics do not deteriorate in three-dimensional problems.

Most of the attention is given to the parameters affecting the acceleration obtained with the multigrid method, including higher-order schemes. The flow characteristics are compared with benchmark or experimental results and provide a solid basis for the conclusions, which are drawn from the present study.

4.1. Cavity case

The recirculating flow inside a lid-driven cavity has been widely used for the assessment of the accuracy and convergence of CFD methods. More details about the flow characteristics in the cavity can be found in the papers of Varonos and Bergeles [3] and Ghia *et al.* [16].

The results presented here include a parametric study for the tuning of the multigrid parameters, namely the number of grid levels and the V-cycle type. The finest grid used is uniform, defined by 65×65 points. There are in total 3–5 grid levels with dimensions 65×65, 33×33, 17×17 and 5×5 points. Two Reynolds numbers have been investigated: 100 and 5000. The study is focused on $Re = 5000$, in which most of convergence and accuracy problems occur. The underrelaxation factors for pressure and momentum equations (equal to 0.5) are the same for both single and multigrid calculations. Iterations are counted on the finest grid level only. The flow field was assumed converged when all normalized residuals were below of 10^{-4}.

The Hybrid discretization scheme is first employed. Table I presents the influence of the number of grid levels and V-cycle type on the convergence speed-up. The Speed-up given in the last column corresponds to the CPU time required for the single grid calculation with the finest grid (65×65 points), over the CPU time used for the multigrid calculations. The runs were made on an IBM Power PC with the RISC 604 processor. Optimum convergence is achieved with five grids, in conjunction with a [2, 2] V-cycle, giving a speed-up ratio of 36.1. However, since the difference with the combination four grids—[3, 3] cycle is small—it is deduced that the latter is satisfactory as well. Figure 5 shows the convergence histories for the single and multigrid algorithms for the optimum combination five grids—[2, 2] V-cycle. It is worthwhile to point out the highly oscillatory convergence of the mass residual, when only the 65×65 grid is used. In Figure 5, the abscissa corresponds to work units, in which the extra CPU time used

Copyright © 2001 John Wiley & Sons, Ltd.

Table I. Cavity case—Hybrid scheme: speed-up factors for $Re = 100$ with the 65×65 uniform grid.

Iterations	Grid levels	V-cycle type	CPU time (s)	Speed-up
1904	1	—	357	—
82	3	[2, 2]	30.5	11.7
33	4	[2, 2]	12.7	28.1
25*	**5**	**[2, 2]**	**9.90**	**36.1**
24	5	$[m+0, m+0]$	14.7	24.2
23	5	$[m+1, m+1]$	10.7	33.4
26	5	$[m+2, m+2]$	11.3	31.7
24	4	$[m+0, m+0]$	14.4	24.9
23	4	$[m+1, m+1]$	10.3	34.7
26	4	$[m+2, m+2]$	10.9	32.7
27	4	[3, 3]	10.0	35.7
27	5	[3, 3]	10.1	35.1

* In this and succeeding tables, bold numbers correspond to the optimum performance.

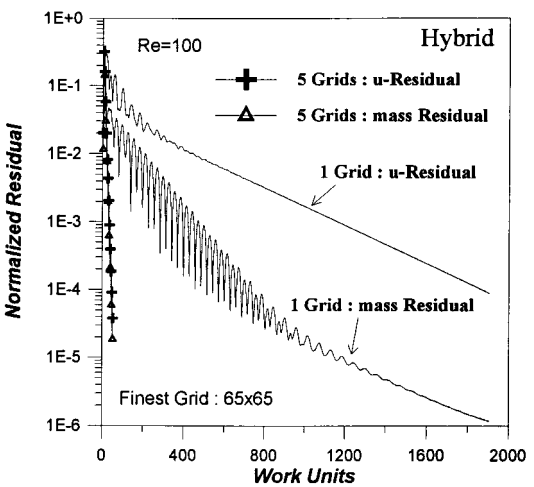

Figure 5. Cavity case with $Re = 100$ (65×65 uniform grid, Hybrid scheme). Convergence history for the u-momentum and mass residuals: full lines = single grid solution; lines with symbols = multigrid solution.

in the multigrid cycle has been accounted for. Therefore, the work units correspond to the exact number of iterations for the single grid calculation only. The representation of the convergence history by means of work units permits the direct deduction of the speed-up obtained with the multigrid method.

The speed-up ratio is non-monotonic with Reynolds number. As the Reynolds number increases, speed-up decreases, and as it is deduced from Table II, for $Re = 5000$ the optimum parameters are three grid levels and $[m + 2, m + 2]$ V-cycle; speed-up is substantially reduced

Copyright © 2001 John Wiley & Sons, Ltd.

Table II. Cavity case—Hybrid scheme: speed-up factors for $Re = 5000$ with the 65×65 uniform grid.

Iterations	Grid levels	V-cycle type	CPU time (s)	Speed-up
927	1	—	175	—
89	3	[2, 2]	32.7	5.3
99	4	[2, 2]	38.0	4.6
91	5	[2, 2]	35.3	4.9
76	5	[3, 3]	27.2	6.4
62	5	$[m+0, m+0]$	38.9	4.5
69	5	$[m+1, m+1]$	31.6	5.5
64	5	$[m+2, m+2]$	27.1	6.4
76	4	[3, 3]	26.8	6.5
67	4	$[m+0, m+0]$	39.9	4.4
75	4	$[m+1, m+1]$	34.9	5.0
67	4	$[m+2, m+2]$	26.5	6.6
73	3	[3, 3]	24.6	7.1
94	3	$[m+0, m+0]$	51.4	3.4
89	3	$[m+1, m+1]$	36.9	4.7
64	**3**	**$[m+2, m+2]$**	**23.9**	**7.3**

and its maximum value is now 7.3. This was, to a degree, anticipated, because from the single grid calculation it is clear that a Reynolds number increase facilitates the solver convergence. This observation is justified by the single-grid iterations number (1904 for $Re = 100$ and 972 for $Re = 5000$) as well as by the convergence history (Figure 6). The reduction in multigrid

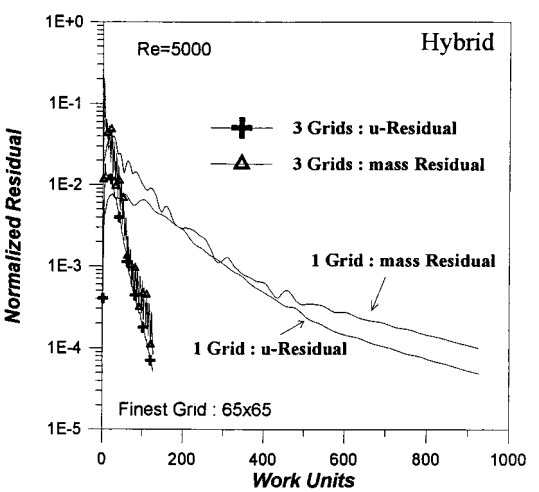

Figure 6. Cavity case with $Re = 5000$ (65×65 grid, Hybrid scheme). Convergence history for the u-momentum and mass residuals: full lines = single grid solution; lines with symbols = multigrid solution.

Copyright © 2001 John Wiley & Sons, Ltd.

efficiency for high Reynolds numbers has also been reported by Lien and Leschziner [8] and Ferziger and Peric [23]. In their studies, the maximum Reynolds number is 1000, for which the speed-up was found equal to 6.2 and 3 respectively, with a 64×64 grid. However, the most important characteristic of the multigrid method is that when very fine grids are used, the speed-up factor increases, because the computational work is roughly proportional to the unknowns number [7]. Figure 7 shows the convergence history for the calculation with a 257×257 uniform grid, including six multigrid levels and a $[m+2, m+2]$ V-cycle. For this computation, the speed-up factor was equal to 48.

4.1.1. Higher-order schemes. Table III summarizes the results concerning the use of the higher-order discretization schemes VONOS and QUICK for $Re = 5000$. The schemes were employed in the dual way mentioned in Section 3.4. From the results it is obvious that this type of flow favours the application of higher-order discretization on all grid levels. Optimum performance for VONOS is achieved with five grids and a [3, 3] V-cycle. The speed-up factor is 9.3 compared with 8.1 when the scheme is used on the finest grid only.

As mentioned in Sections 1 and 3.4, the most important conclusion of the present study is that the multigrid method stabilizes the convergence characteristics of unbounded higher-order schemes. Figure 8 shows that the calculation with the QUICK scheme for $Re = 5000$ does not converge. On the contrary, when the multigrid cycles are activated, convergence is even faster than the one of VONOS (Table III). It is also worthwhile to note that, when QUICK is activated at all grid levels, the required time for convergence is reduced by a factor of 2.4 compared with the calculation where QUICK is employed on the finest grid only.

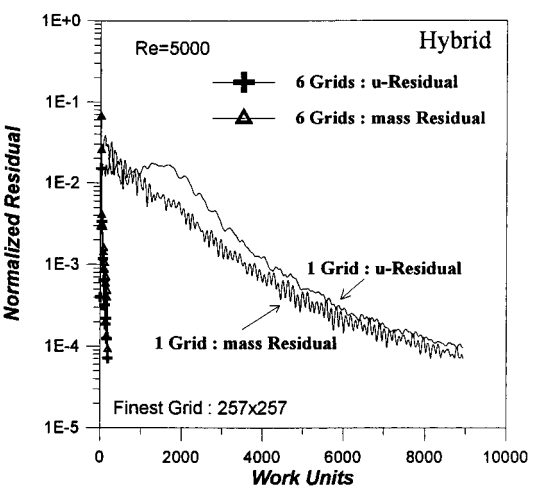

Figure 7. Cavity case with $Re = 5000$ (257×257 grid, Hybrid scheme). Convergence history for the u-momentum and mass residuals: full lines = single grid solution; lines with symbols = multigrid solution.

Copyright © 2001 John Wiley & Sons, Ltd.

Table III. Cavity case—VONOS–QUICK schemes: speed-up factors for $Re = 5000$ with the 65×65 uniform grid.

Iterations	Grid levels	V-cycle type	Scheme	CPU time (s)	Speed-up
5419	1	—	VONOS	1473	—
586	3	$[m+2, m+2]$	VONOS	285.5	5.2
742	3	[3, 3]	VONOS	331.3	4.4
385	4	$[m+2, m+2]$	VONOS	196.4	7.5
466	4	[3, 3]	VONOS	223.1	6.6
346	5	$[m+2, m+2]$	VONOS	182.9	8.1
394	5	[3, 3]	VONOS	182.3	8.1
274	5	$[m+2, m+2]$	VONOS (all grid levels)	166.7	8.8
289	**5**	**[3, 3]**	**VONOS (all grid levels)**	**157.9**	**9.3**
Not converged	1	—	QUICK	—	—
223	5	$[m+2, m+2]$	QUICK	107.6	Not defined
97	5	[3, 3]	QUICK (all grid levels)	47.03	Not defined
82	**5**	**$[m+2, m+2]$**	**QUICK (all grid levels)**	**44.30**	**Not defined**

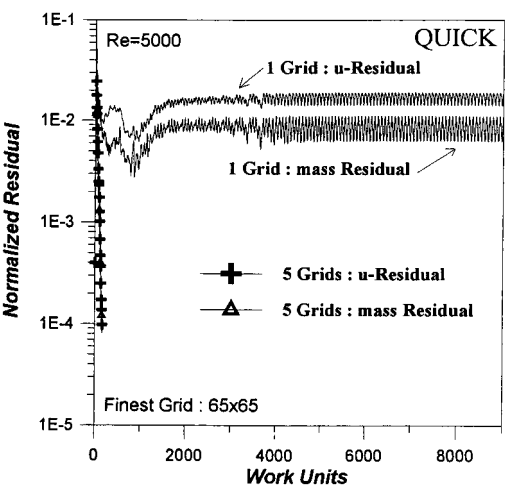

Figure 8. Cavity case with $Re = 5000$ (65×65 grid, QUICK scheme applied on all grid levels). Convergence history for the u-momentum and mass residuals: full lines = single grid solution; lines with symbols = multigrid solution.

Copyright © 2001 John Wiley & Sons, Ltd.

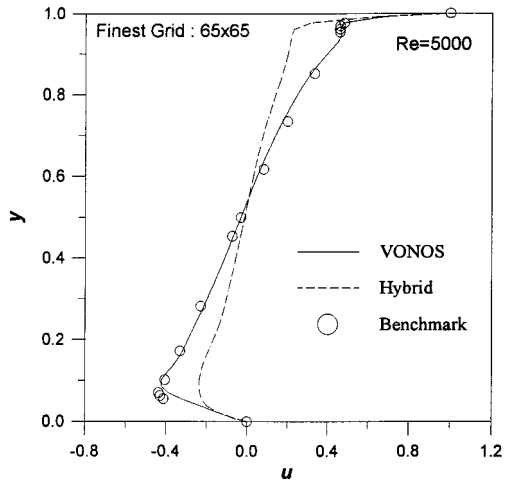

Figure 9. Comparison of the u velocity profiles along the vertical centreline of the cavity obtained with the Hybrid and VONOS schemes (65×65 grid) against the benchmark solution for $Re = 5000$.

Figures 9 and 10 present the comparison of the velocity profiles at the geometrical centreline of the cavity for Hybrid, VONOS and QUICK schemes. In Figure 9 it is clear that the divergence of the profile predicted with the Hybrid scheme from the data of Ghia *et al.* [16] is

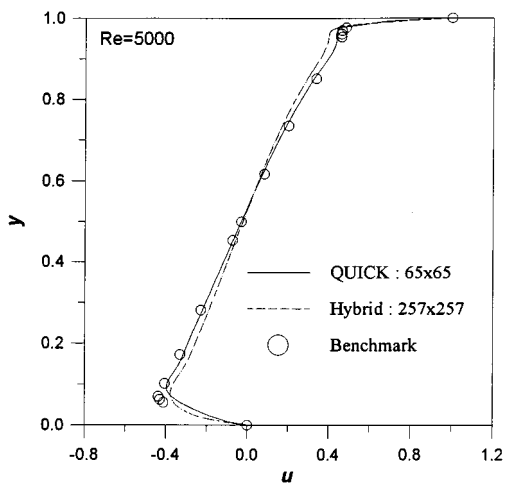

Figure 10. Comparison of the u velocity profiles along the vertical centreline of the cavity obtained with the Hybrid (257×257 grid) and QUICK schemes (65×65 grid) against the benchmark solution for $Re = 5000$.

Copyright © 2001 John Wiley & Sons, Ltd.

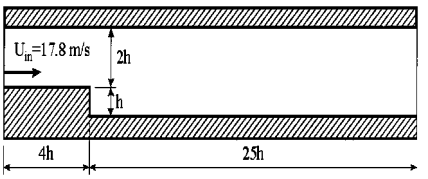

Figure 11. Geometrical arrangement for the flow over the two-dimensional backward-facing step.

quite significant due to the increased numerical diffusion this scheme introduces into the numerical solution [4]. On the other hand, VONOS matches very well the benchmark data, although the computational grid is uniform and rather coarse for this type of flow. The same observation is made in Figure 10, where the Hybrid scheme fails to describe the velocity profile, even when a 257×257 grid is used. It is important to note that QUICK gives a more accurate profile employing only 6.4 per cent of the discretization points used to obtain the solution with the Hybrid scheme.

4.2. Step case

The geometry of the two-dimensional flow in a backward-facing step is shown in Figure 11. It has been experimentally investigated by Kim *et al.* [17]. The Reynolds number is $Re = (U_{in}h)/\nu = 69\,600$, with $U_{in} = 17.8\ \mathrm{m\,s^{-1}}$ and $h = 0.0381$ m. The fluid density and dynamic viscosity are $\rho = 1.886\ \mathrm{kg\,m^{-3}}$ and $\mu = 1.837 \times 10^{-5}\ \mathrm{kg\,m^{-1}\,s^{-1}}$ respectively. The inlet velocity and k profiles measured by Kim *et al.* [17] were used as inlet conditions. The underrelaxation factors for the momentum and pressure equations are common for the single and multigrid procedure and were equal to 0.3. The convergence criterion is met at 10^{-4} for all normalised residuals.

Table IV summarizes the results obtained with the Hybrid and QUICK schemes on a 65×65 non-uniform grid. Speed-up (only the maximum is reported) is equal to 2.9 for both schemes and it was achieved with three grid levels and a $[m+4, m+1]$ V-cycle. In contrast to the lid-driven cavity case, the application of QUICK on all grid levels did not improve substantially the convergence characteristics and in terms of computational time, the speed-up is practically the same.

Table IV. Step case—Hybrid–QUICK schemes: speed-up factors for the 65×65 non-uniform grid.

Iterations	Grid levels	V-cycle type	Scheme	CPU time (s)	Speed-up
2578	1	—	Hybrid	639	—
606	**3**	**[*m*+4, *m*+1]**	**Hybrid**	**218**	**2.9**
2760	1	—	QUICK	822	—
686	**3**	**[*m*+4, *m*+1]**	**QUICK**	**284**	**2.9**
611	**3**	**[*m*+4, *m*+1]**	**QUICK (all grid levels)**	**276**	**3.0**

Copyright © 2001 John Wiley & Sons, Ltd.

Figure 12 shows the convergence histories for QUICK. The main feature in this figure is that, in the beginning of the calculation, the normalized residuals are two orders of magnitude higher than those of the single grid calculation. This is possibly due to the fact that the calculation started with a non-zero field, which was estimated according to the inlet conditions. Nevertheless, it is obvious that the dependence of the flow field on the $k-\varepsilon$ turbulence model has substantially decreased the convergence acceleration of the multigrid method. Figure 13 presents the convergence history for the 257×129 non-uniform grid. The multigrid calculation was performed using four grids and a $[m+4, m+1]$ V-cycle, without using higher-order discretization on the coarse grids; the speed-up factor was equal to 13.8.

Figures 14 and 15 present some features of the field, namely the *Cp* along the 'ground' after the step and two characteristic u and k profiles, compared with the measurements of Kim *et al.* [17] and the predictions of Sohn [26].

4.3. Cube case

The turbulent flow around a wall-mounted cube (Figure 16) has been simulated in order to investigate the efficiency of the multigrid method—integrated into the SIMPLE algorithm—when it is applied to a complex three-dimensional case. The velocity and pressure distributions on the cube faces, as well as the inlet profiles, were measured by Castro and Robins [18]. The Reynolds number is $Re = (U_{\text{in}}h)/\nu = 4000$, with $U_{\text{in}} = 0.5\ \text{m s}^{-1}$ and $h = 0.2$ m (cube height). The boundary layer thickness is equal to $10h$. The fluid density and dynamic viscosity are $\rho = 1.188\ \text{kg m}^{-3}$ and $\mu = 1.798 \times 10^{-5}\ \text{kg m}^{-1}\,\text{s}^{-1}$. The underrelaxation factors for the

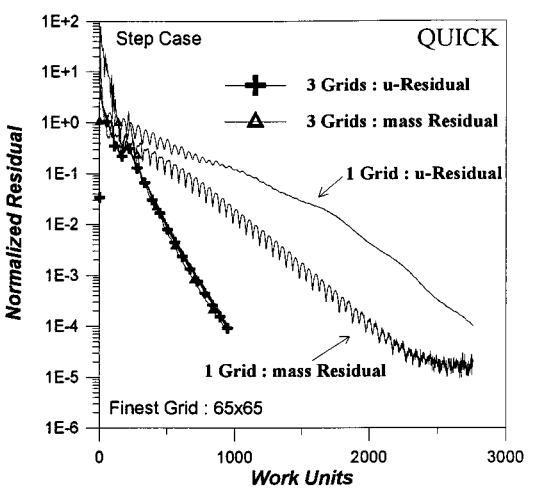

Figure 12. Step case (65×65 grid, QUICK scheme). Convergence history for the u-momentum and mass residuals: full lines = single grid solution; lines with symbols = multigrid solution.

Copyright © 2001 John Wiley & Sons, Ltd.

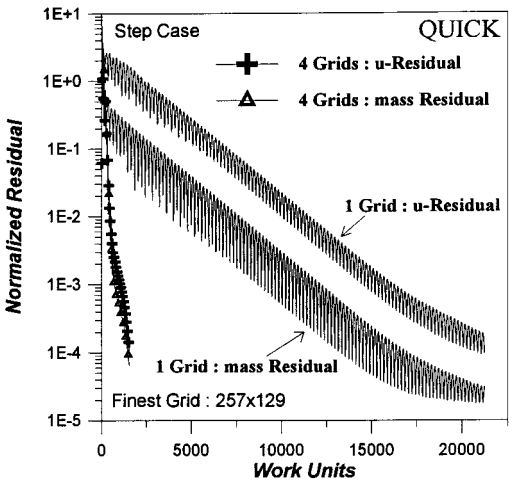

Figure 13. Step case (257×129 grid, QUICK scheme). Convergence history for the u-momentum and mass residuals: full lines = single grid solution; lines with symbols = multigrid solution.

momentum and pressure equations were all equal to 0.3. The convergence criterion was set again at 10^{-4} for all normalized residuals.

Two different non-uniform grids were used for the calculations; a $65 \times 65 \times 33$ and a $81 \times 81 \times 41$ points (Figure 17). Hybrid and QUICK schemes were employed on the coarse grid (the $65 \times 65 \times 33$ one), whereas for the fine one only the QUICK has been used. Figures 18–20 present the convergence history of each run. Due to the increased memory requirements,

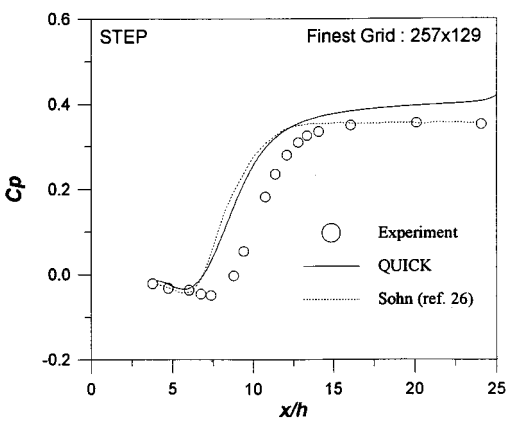

Figure 14. Step case (257×129 grid, QUICK scheme). Cp distribution on the lower wall (after the step): comparison with the experimental data and the predictions of Sohn [26].

Copyright © 2001 John Wiley & Sons, Ltd.

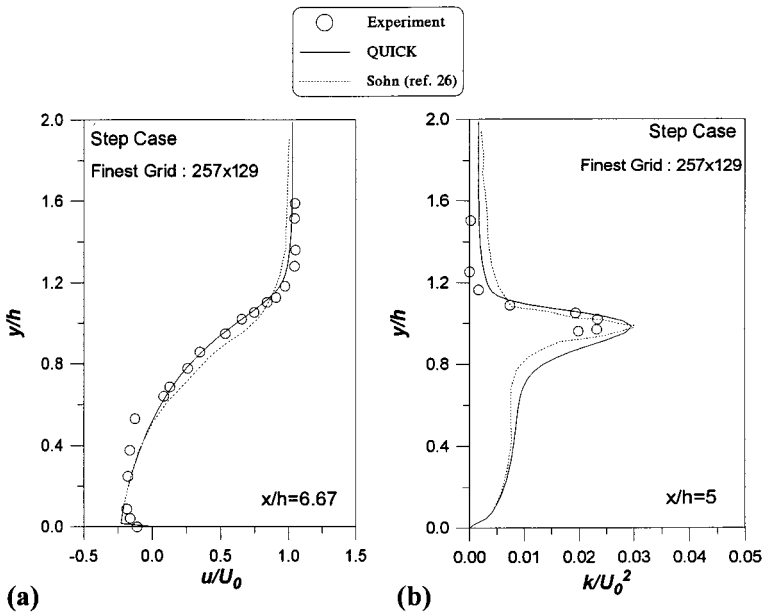

Figure 15. Step case (257×129 grid, QUICK scheme). Comparison with the experimental data and the predictions of Sohn [26]: (a) u velocity at $x/h = 6.67$, (b) turbulent kinetic energy k at $x/h = 5$.

the calculations were performed on a DEC Alpha (Personal Workstation) with the 500 series processor; for the calculation with the $81 \times 81 \times 41$ grid, 80 Mb of RAM were required. The work units on Figures 18–20 show that the speed-up factors for the $65 \times 65 \times 33$ grid are equal to 2.3 and 2.5 for the Hybrid and QUICK respectively. The speed-up factor for the finer $81 \times 81 \times 41$ grid is, as expected, higher and equal to 2.7. All calculations were made using three grid levels and a $[m+2, m+2]$ V-cycle. For this case a relaxation on the coarse grid

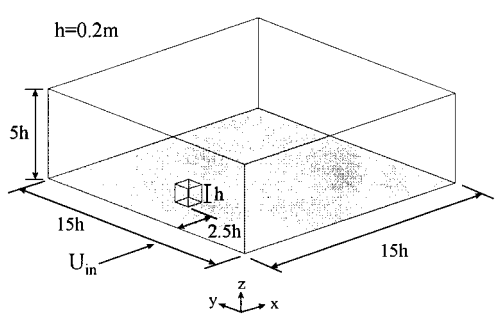

Figure 16. Geometrical arrangement for the flow around the wall mounted cube.

Copyright © 2001 John Wiley & Sons, Ltd.

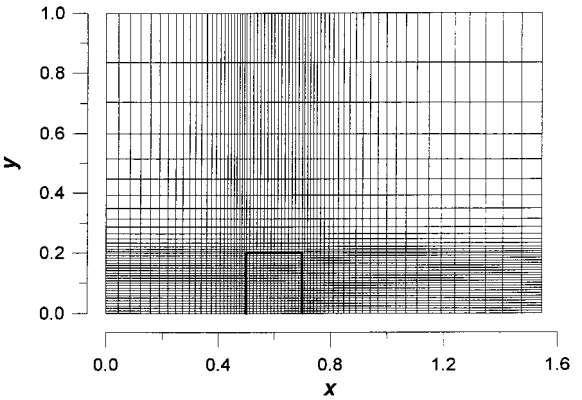

Figure 17. Cube case. Detail of the 257×129 grid around the cube.

pressure correction has been also introduced and its value was set to 0.1. These multigrid parameters have been tuned after an extended optimisation study, which was conducted on coarser grids and was similar to the one carried out for the lid-driven cavity case. The study showed that the application of higher-order discretization on all grid levels for complex high Reynolds number three-(and two-)dimensional cases should be avoided. This is due to the fact that convergence characteristics are only slightly improved, whereas additional computational time is consumed by the higher-order scheme on the coarser grids. Finally, in the frame of the

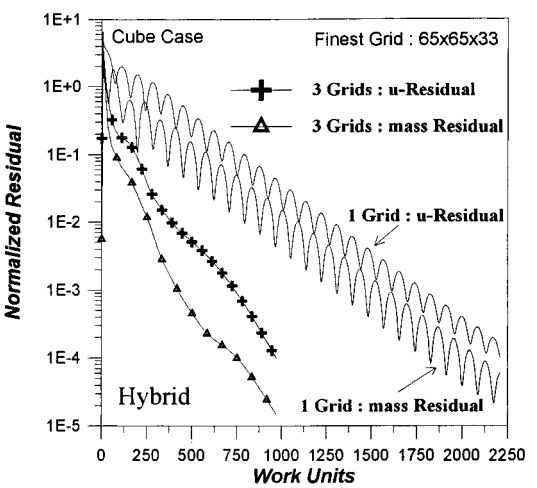

Figure 18. Cube case ($65 \times 65 \times 33$ grid, Hybrid scheme). Convergence history for the u-momentum and mass residuals: full lines = single grid solution; lines with symbols = multigrid solution.

Copyright © 2001 John Wiley & Sons, Ltd.

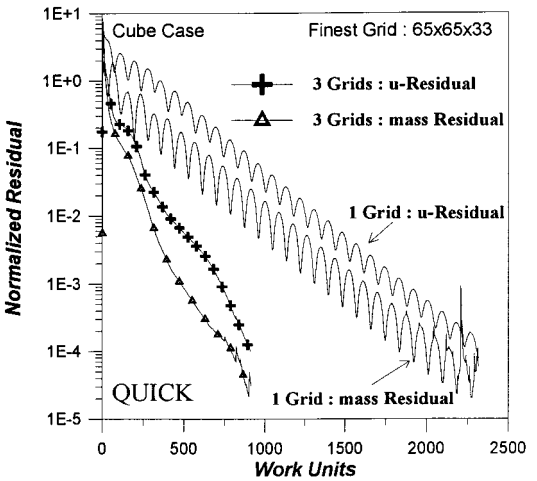

Figure 19. Cube case ($65 \times 65 \times 33$ grid, QUICK scheme). Convergence history for the u-momentum and mass residuals: full lines = single grid solution; lines with symbols = multigrid solution.

above study, it was also found that multigrid acceleration is reduced, as the grid non-uniformity is increased.

4.3.1. Flow field characteristics. The flow field around the wall-mounted cube has also been investigated by Baetke *et al.* [27] and Murakami *et al.* [28]. Figure 21 presents the pressure

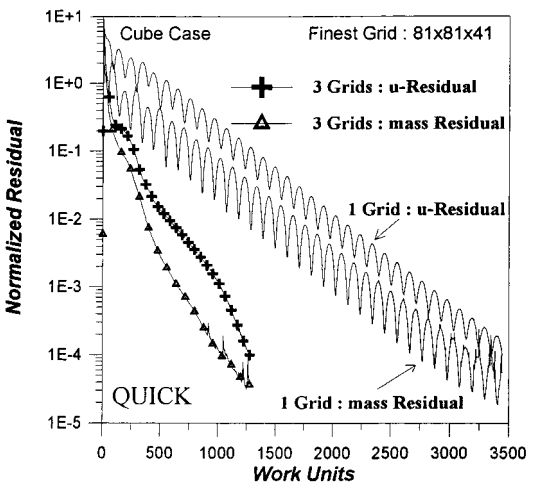

Figure 20. Cube case ($81 \times 81 \times 41$ grid, QUICK scheme). Convergence history for the u-momentum and mass residuals: full lines = single grid solution; lines with symbols = multigrid solution.

Copyright © 2001 John Wiley & Sons, Ltd.

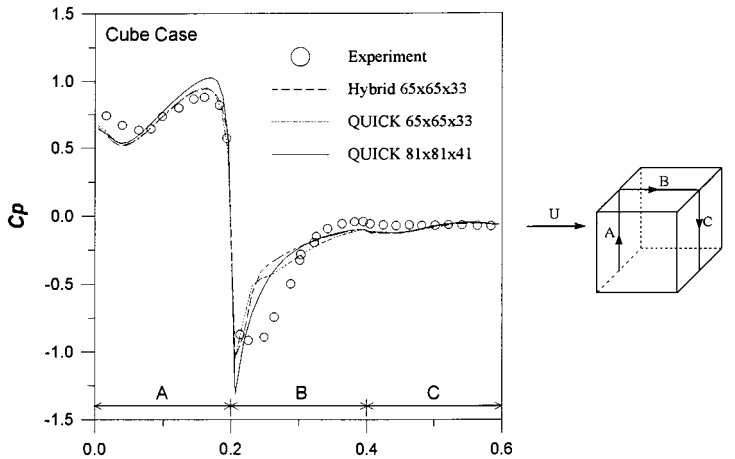

Figure 21. Cube case. *Cp* distribution on x–z plane for cube sides A, B and C: comparison with the experimental data.

coefficient (*Cp*) distribution on the cube in the x–z plane. Most discrepancies occur in the beginning of sides A and B due to the well-known inability of the k–ε model to accurately predict the size of recirculatimg flow in these areas. In this figure it is also clear that QUICK gives more accurate results than the Hybrid scheme when the $65 \times 65 \times 33$ grid is used. The

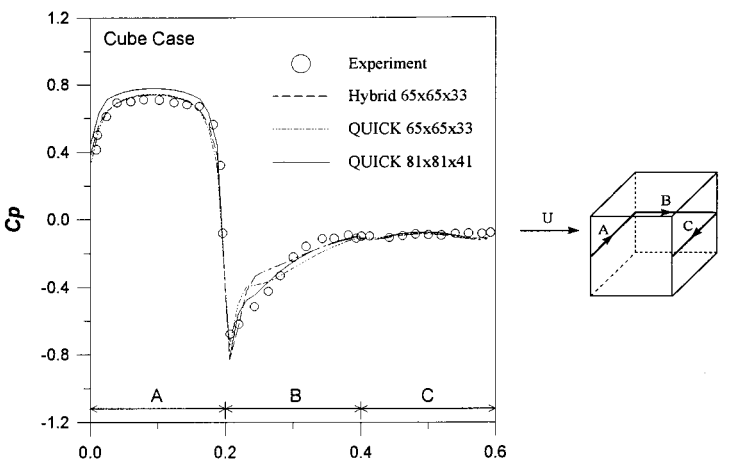

Figure 22. Cube case. *Cp* distribution on x–y plane for cube sides A, B and C: comparison with the experimental data.

Copyright © 2001 John Wiley & Sons, Ltd.

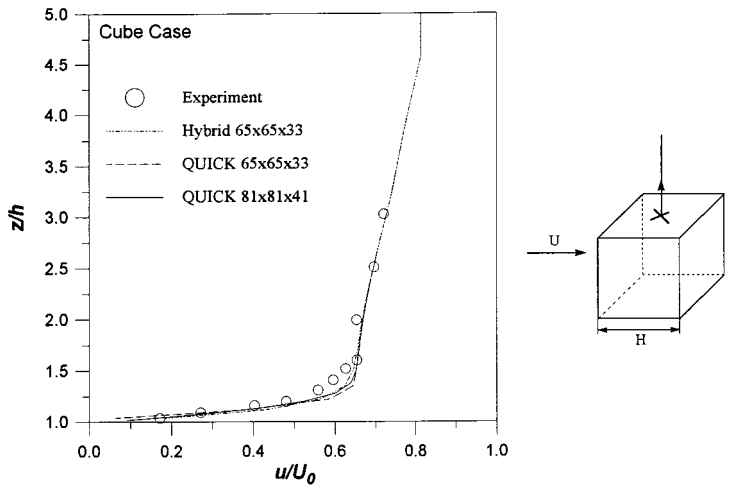

Figure 23. Cube case. Vertical u velocity profiles along x–z plane, starting from the top centre of the cube: comparison with the experimental data.

$81 \times 81 \times 41$ grid calculation (QUICK) presents slightly higher discrepancies close to the end of side A, but gives better predictions in the beginning of side B. According to the investigations of Murakami *et al.* [28], the recirculation bubble in this area can be accurately predicted only by means of large eddy simulation (LES) or direct numerical simulation (DNS) computations.

Figure 22 shows the *Cp* distribution on the x–y plane. The agreement with the experimental data is better in the whole range of the curve. The most accurate predictions are those of the $81 \times 81 \times 41$ grid (QUICK) except side A, where a slight overestimation occurs. As far as the

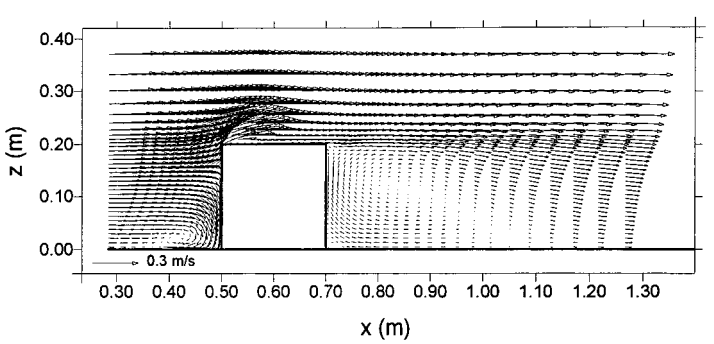

Figure 24. Velocity vectors on the plane crossing the centreline of the cube.

Copyright © 2001 John Wiley & Sons, Ltd.

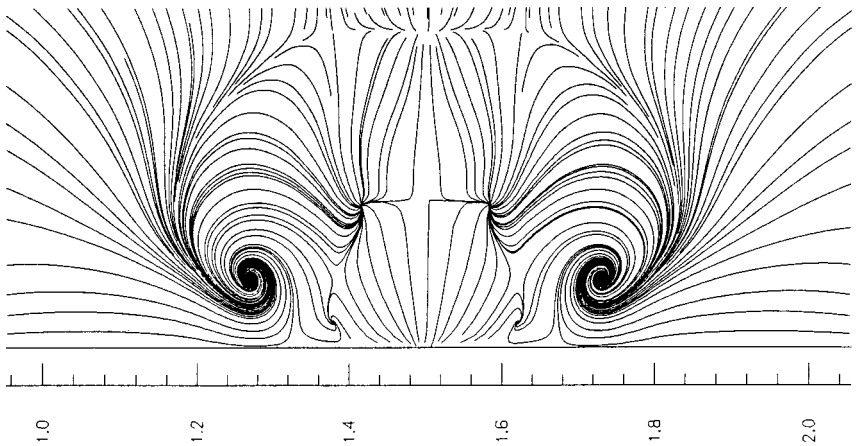

Figure 25. Streamlines on the $y-z$ plane at $0.1h$ downstream of the cube.

velocity field predictions are concerned, from Figure 23 it is obvious that the curves resulting from the three runs almost coincide and agree very well with the experimental data.

Finally, Figures 24 and 25 present one horizontal and one transverse cut of the flow field, where the main patterns of the flow are clearly visualized. The main characteristic of the plane located at $0.1h$ downstream the cube (Figure 25) is the presence of a horseshoe vortex, which is generated due to the vorticity produced along the edges of the cube.

5. CONCLUSIONS

The implementation of the multigrid method into the SIMPLE algorithm showed that it offers important convergence speed-up not only with first-order or bounded discretization schemes, but with higher-order unbounded schemes as well. The multigrid procedure presented in this paper is fully conservative, including a special treatment for the $k-\varepsilon$ equations. Higher-order schemes were employed in a dual approach that considers the application of higher-order discretization whether on all grid levels or the finest grid only. The simulation of three different test cases proved that, in most problems, the application of higher-order schemes results in increased speed-ups compared with first-order (or hybrid) discretization.

According to the numerical results, there is important convergence acceleration, which increases with the grid discretization density. The results indicate that it is favourable to use the QUICK discretization scheme at all cases. In laminar two-dimensional cases, higher-order schemes should be used at all grid levels, whereas for high Reynolds number two- and three-dimensional flows, higher-order discretization is favourable when applied on the finest grid only. In terms of computational time, the multigrid method is 3–4 times faster than the single grid algorithm, for most convection-dominated engineering applications.

Copyright © 2001 John Wiley & Sons, Ltd.

REFERENCES

1. Leonard BP. A stable and accurate convective modeling procedure based on quadratic interpolation. *Computer Methods in Applied Mechanics and Engineering* 1979; **19**: 59–98.
2. Gaskell PH, Lau AKC. Curvature-compensated convective transport: SMART, a new boundedness-preserving transport algorithm. *International Journal for Numerical Methods in Fluids* 1988; **8**: 197–210.
3. Varonos A, Bergeles G. Development and assessment of a variable order non oscillatory scheme for convection terms discretisation. *International Journal for Numerical Methods in Fluids* 1998; **26**: 1–16.
4. Papadakis G, Bergeles G. A locally modified second order upwind scheme for convection terms discretization. *International Journal for Numerical Methods for Heat and Fluid Flows* 1995; **5**: 49–62.
5. Fletcher R. Conjugate gradient methods for indefinite systems. In *Proceedings of the Dundee Conference on Numerical Analysis*, *Lecture Series in Mathematics*, Watson GA (ed.). Springer: Berlin, 1976; 506.
6. Meijerink JA, Van der Vorst HA. Guidelines for the usage of incomplete decomposition in solving sets of linear equations as they occur in practical problems. *Journal of Computational Physics* 1981; **44**: 134–155.
7. Hackbusch W. *Multi-Grid Methods and Applications*. Springer: Berlin, 1985.
8. Lien FS, Leschziner MA. Multigrid acceleration for turbulent flow with a non-orthogonal collocated scheme. *Journal of Computer Methods in Applied Mechanics and Engineering* 1994; **118**: 351–371.
9. Smith DM, Gosman AD. An application of multigrid with local grid refinement on fluid flow calculations. In *Proceedings of the 5th Copper Mountain Conference on Multigrid Methods*, Copper Mountain, CO, McCormick SF, Mandel J (eds), 1991.
10. Vanka SP. Block-implicit multigrid solution of Navier–Stokes equations in primitive variables. *Journal of Computational Physics* 1986; **65**: 138–158.
11. Sivaloganathan S, Shaw GJ. A multigrid method for recirculating flows. *International Journal for Numerical Methods in Fluids* 1988; **8**: 417–440.
12. Patankar SV, Spalding DB. A calculation procedure for heat, mass and momentum transfer in three-dimensional parabolic flows. *International Journal of Heat and Mass Transfer* 1972; **15**: 1787–1806.
13. Dick E, Steelant J. Coupled solution of the steady compressible Navier–Stokes equations and the k–ε turbulence equations with a multigrid method. *Applied Numerical Mathematics* 1997; **23**: 49–61.
14. Drikakis D, Iliev OP, Vassileva DP. A nonlinear multigrid method for the three-dimensional incompressible Navier–Stokes equations. *Journal of Computational Physics* 1998; **146**: 301–321.
15. Oosterlee CW, Gaspar FJ, Washio T, Wienands R. Multigrid line smoothers for higher order upwind discretizations of convection-dominated problems. *Journal of Computational Physics* 1998; **1**: 274–307.
16. Ghia U, Ghia KN, Shin CT. High-*Re* solutions for incompressible flow using the Navier–Stokes equations and a multigrid method. *Journal of Computational Physics* 1982; **48**: 387–411.
17. Kim J, Kline SJ, Johnston JP. Investigation of a reattaching turbulent shear layer: flow over a backward-facing step. *Transactions of the ASME* 1980; **102**: 302–308.
18. Castro IP, Robins AG. The flow around a surface-mounted cube in uniform and turbulent streams. *Journal of Fluid Mechanics* 1977; **79**: 307–335.
19. Launder BE, Spalding DB. The numerical computation of turbulent flows. *Computer Methods in Applied Mechanics and Engineering* 1974; **3**: 269–289.
20. Leonard BP, Mokhtari S. Beyond first order upwinding: the ULTRA-SHARP alternative for non-oscillatory steady state simulation of convection. *International Journal for Numerical Methods in Engineering* 1990; **30**: 729–766.
21. Rhie C, Chow W. Numerical study of the turbulent flow past an airfoil with trailing edge separation. *AIAA Journal* 1983; **21**: 1525–1532.
22. Hortmann M, Peric M, Scheuerer G. Finite volume multigrid prediction of laminar natural convection: benchmark solutions. *International Journal for Numerical Methods in Fluids* 1990; **11**: 189–207.
23. Ferziger J, Peric M. *Computational Methods for Fluid Dynamics*. Springer: Berlin, 1997.
24. Hänel D, Schröder W, Seider G. Multigrid methods for the solution of the compressible Navier–Stokes equations. In *Proceedings of the 4th GAMM Seminar 'Robust Multi-Grid Methods*, Hackbusch W (ed.). Vieweg: Wiesbaden, 1988; 114–127.
25. Spalding DB. A novel finite difference formulation for differential expressions involving both first and second order derivatives. *International Journal for Numerical Methods in Engineering* 1972; **4**: 551–559.
26. Sohn JL. Evaluation of FIDAP on some classical laminar and turbulent benchmarks. *International Journal for Numerical Methods in Fluids* 1988; **8**: 1469–1490.
27. Baetke F, Werner H, Wengle H. Numerical simulation of turbulent flow over surface-mounted obstacles with sharp edges and corners. *Journal of Wind Engineering and Industrial Aerodynamics* 1990; **35**: 129–147.
28. Murakami S, Mochida A, Hayashi Y. Examining k–e model by means of a wind tunnel test and large-eddy simulation of the turbulence structure around a cube. *Journal of Wind Engineering and Industrial Aerodynamics* 1990; **35**: 87–100.

Copyright © 2001 John Wiley & Sons, Ltd.